



Capping technique for chemical vapor deposition of large and uniform MoS₂ flakes

Menelaos Tsigkourakos^{a,*}, Maria Kainourgiaki^a, Evangelos Skotadis^a,
Konstantinos P. Giannakopoulos^b, Dimitris Tsoukalas^a, Yannis S. Raptis^a

^a Department of Applied Physics, National Technical University of Athens, Heroon Polytechniou 9, 15780, Athens, Greece

^b Institute of Nanoscience and Nanotechnology, National Center for Scientific Research "Demokritos", Patriarchou Gregoriou E & Neapoleos 27, 15341, Athens, Greece

ARTICLE INFO

Keywords:

Two-dimensional materials
Molybdenum disulfide growth
Chemical vapor deposition
Large flakes
Homogeneous deposition

ABSTRACT

Molybdenum disulfide (MoS₂) has attracted a lot of attention due to its semiconducting behavior. Chemical vapor deposition of MoS₂ is considered a relatively simple and user-friendly technique but there are several obstacles that may hinder the growth, and might result in rather small and non-uniformly distributed triangular flakes over the substrate surface. To tackle this issue, we developed an approach for large flakes (>300 μm) grown homogeneously over two substrates at once. This is based on spin-coating one of the two substrates with an aqueous solution of Mo-based salt particles, and covering it with the other. During the growth, the particles will act as nucleation sites for both substrates. Raman and atomic force microscopy measurements show that the grown flakes are monolayer. Finally, electrical measurements demonstrate the semiconducting behavior of the material and further analysis reveal two conduction mechanisms (nearest-neighbor and variable-range hopping) that dominate according to the temperature.

1. Introduction

Molybdenum disulfide (MoS₂) is a two-dimensional (2D) material that belongs to the group of layered transition metal dichalcogenides. It presents a large number of interesting electrical [1,2], optical [3,4] and mechanical [5,6] properties which make it a very attractive material on several different applications such as transistors [7,8], sensors [9–11] and thermoelectric generators [12] among others. The main synthesis methods to grow such a material are mechanical [13] and/or chemical [14] exfoliation, as well as chemical vapor deposition (CVD) [15]. The latter method is preferred and most widely used nowadays, since it offers a large-area deposition with a controlled quality and thickness of the synthesized MoS₂ [16,17]. However, this technique suffers from reproducibility, due to the multiple input parameters that determine the growth result of each CVD system, such as precursor materials, temperature, pressure, reaction time, gas flow rate etc. Moreover, the values of the aforementioned parameters might differ dramatically on different CVD systems and are influenced by the geometrical characteristics of each setup.

The most commonly used solid precursors for MoS₂ CVD growth are molybdenum trioxide (MoO₃) and sulfur (S). A major issue when using

MoO₃ is that the location of the formed MoS₂ flakes is dependent on the relative distance among the substrate-MoO₃-S [18,19] and are not been uniformly formed over the substrate surface [20], resulting in regions with no growth at all and regions of multilayer/bulk MoS₂. Specifically, the region of the substrate surface that the growth (i.e. large monolayer MoS₂ flakes) is observed, is usually at the edges of the substrate. This can be crucial when devices or certain configurations need to be formed based on the location of such flakes without any further transfer of the 2D material. Moreover, the usage of MoO₃ undermines several other difficulties such as poisoning of the precursor material (i.e. sulfurization of the MoO₃ powder which prevent the precursor's sublimation), and deposition of MoO_x phases over the substrate which suppress the formation of MoS₂, among others. Many groups have tackled these problems using seeding promoters [21] or liquid precursors [22,23] which on the other hand, require additional precursor elements (such as perylene-3,4,9,10-tetracarboxylic acid tetrapotassium salt) and the uniformity of the formed MoS₂ flakes over the substrate surface is not always guaranteed.

Recent studies showed that the partial coverage of the substrate during the growth process allows a uniform formation of monolayer MoS₂ (as well as other 2D materials) over the substrate surface [24,25].

* Corresponding author.

E-mail address: mxtsig@central.ntua.gr (M. Tsigkourakos).

<https://doi.org/10.1016/j.tsf.2021.138808>

Received 9 December 2020; Received in revised form 18 June 2021; Accepted 23 June 2021

Available online 27 June 2021

0040-6090/© 2021 Elsevier B.V. All rights reserved.

Mohapatra et al. [26] explained this phenomenon due to the increased vapor sulfur pressure rate compared to MoO_3 , which flushes out MoO_3 molecules of the covered region. However, the use of MoO_3 still results in a lack of reproducibility among different CVD systems and thus, a global recipe for massive and reproducible CVD growth of MoS_2 is yet missing.

In this work, we present a substrate capping technique for reproducible formation of MoS_2 over two substrate pieces at once (the original and the dummy substrate that covers the former). The proposed synthesis method is based on the combination of a liquid precursor ($\text{Na}_2\text{MoO}_4 \cdot \text{H}_2\text{O}$) as the Mo-based precursor material (spin-coated over one deposition surface), and the sandwiching of two deposition surfaces that are used for MoS_2 growth. The physical contact of the two pieces allows both of the substrates to share the Mo-based salt particles which in turn, act as nucleation centers. Thus, this method offers a pair of uniformly and fully covered MoS_2 -deposited substrates at once, with large triangular-shaped flakes of larger than $300 \mu\text{m}$ in size. The produced MoS_2 is a monolayer, as shown by our Raman and atomic force microscopy (AFM) measurements, and exhibits semiconducting behavior, as shown by our low-temperature electrical characterization. Finally, a further analysis and interpretation of our electrical data reveals two different conduction mechanisms of the 2D material, according to the temperature.

2. Experimental details

2.1. Synthesis of MoS_2

Sodium molybdate (Na_2MoO_4 , Sigma Aldrich ($\geq 98\%$ purity)) is diluted in deionized (DI) water in order to prepare a solution of 2 mg/mL concentration. Additionally, two $2 \times 2 \text{ cm}^2$ pieces of Si/SiO_2 (300 nm) are cleaned using a Piranha solution ($\text{H}_2\text{SO}_4:\text{H}_2\text{O}_2$ 3:1) for 30 min, rinsed with DI water and dried with N_2 . One of these two pieces is then spin-coated with the aqueous solution at 2000 rpm for 2 min. This piece will be hereafter named as “original substrate (OS)”. Next, the non-coated piece (dummy substrate, DS) is placed on top of OS and the sandwiched substrates are placed inside the quartz tube of a tubular oven (Carbolite, TZF 12/65/550); sulfur (S, Sigma Aldrich (99.998% purity)) is also added in the oven, inside an alumina boat. The distance of the substrates and S is 15 cm . Once both substrates and alumina boat with S are loaded into the quartz tube and the latter is sealed, the oven is heated up to $150 \text{ }^\circ\text{C}$ for 1 hr with a constant flow of N_2 at 1000 sccm . Then, the temperature is increased up to $900 \text{ }^\circ\text{C}$ with a rate of $15 \text{ }^\circ\text{C}/\text{min}$ and kept at this value for 5 min, while the N_2 flow rate is set to 50 sccm . Finally, the quartz tube is cooled off rapidly by setting the temperature value at room temperature and pulling the tube outside the tubular oven.

2.2. Electrode formation

Ti (4 nm)/Au (40 nm) electrodes are deposited using an electron-beam evaporation system (Mantis, QUAD Series). Patterning and formation of the electrodes is achieved using optical lithography together with a mask aligner, and the lift-off technique.

2.3. Characterization

The deposited MoS_2 is characterized using scanning electron microscopy (SEM, FEI, Nova NanoSEM230) at an accelerating voltage of 10 kV , in order to study the morphology of the grown material and measure the size of the formed triangular flakes. Moreover, the thickness of the flakes are measured using atomic force microscopy (AFM, Veeco, di Innova) at non-contact (tapping) mode, as well as Raman spectroscopy (Horiba, T64000 triple monochromator). Finally, low temperature electrical measurements (down to 80 K) are performed using a cryostat probe station with two probes (Janis Ltd., ST-500-1-(2CX)).

3. Results and discussion

3.1. Growth of large MoS_2 triangular flakes

Fig. 1 shows the preparation and configuration of the “sandwiched substrates” that are used in this work. As can be seen in Fig. 1(a), only the OS is pretreated by spin-coating the aqueous solution ($\text{Na}_2\text{MoO}_4 \cdot \text{H}_2\text{O}$), which will result in uniformly ordered Mo-based salt particles over the substrate surface (as shown by the SEM inset image). Then, the clean DS is placed on top of the OS spin-coated side (see Fig. 1(b)). Finally, the sandwiched substrates are placed inside the quartz tube of the tubular oven, together with the S-containing alumina boat (see Fig. 1(c)). At this point, it should be noted that a reference sample that is not sandwiched (but spin-coated following the same procedure) is also placed inside the oven. During the growth process, the inert gas (N_2) will carry the S vapors towards the substrates, where the sulfuration of the Mo-based particles will take place at $900 \text{ }^\circ\text{C}$. Different amounts of S ($300, 400$ and 600 mg) have been tested with no significant differences in the result of the growth process. Therefore, 300 mg of S has been used in every growth run reported in this work. Fig. 2 shows SEM images of the grown MoS_2 over both OS and DS at a random location of each piece, whereby large (from $150 \mu\text{m}$ up to $>300 \mu\text{m}$, see Fig. 2(a)) triangular flakes and at a relatively uniform order (Fig. 2(c) and (d)) are visible. Both pieces demonstrate similar flakes in terms of size and quantity, exhibiting no significant differences on various locations, which indicates a homogeneous growth over their entire surface. The reference sample demonstrates small flakes ($<20 \mu\text{m}$, Fig. 2(b)) with irregular shapes, indicating that the concentration and flow rate of the precursor gasses significantly change, close to the surface of the sandwiched substrates. Therefore, the use of the liquid precursor results in a flake-based layer of high density but with small and irregular shapes. However, the combination of the liquid precursor with the capping method, which changes the concentration of the precursor gasses at the substrate surface region, results in large and uniform MoS_2 flakes.

3.2. Raman and AFM characterization

Raman spectroscopy and AFM characterization are performed on both OS and DS pieces, showing similar results. During Raman

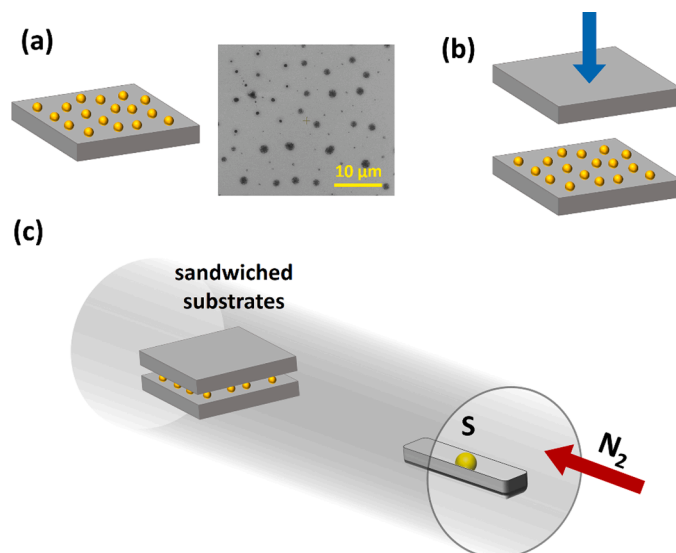


Fig. 1. (a) Schematic and SEM image of the original substrate (OS) after being spin-coated with $\text{Na}_2\text{MoO}_4 \cdot \text{H}_2\text{O}$ solution, (b) a clean dummy substrate (DS) is placed on top of the OS forming sandwiched substrates, (c) sandwiched substrates and the alumina boat containing S are located inside the quartz tube of the oven.

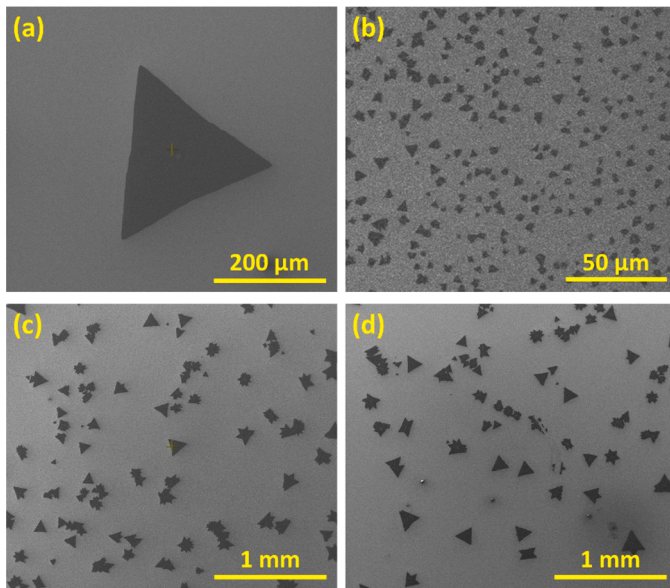


Fig. 2. SEM image (a) of a large triangular flake ($>300 \mu\text{m}$) grown over OS, and (b) of the reference sample. Lower magnification SEM image of (c) OS and (d) DS surface.

measurements, a 532 nm laser line has been used with a laser intensity of 0.2 mW. Fig. 3 shows two Raman spectra of flakes from both OS and DS. Two vibrational modes are clearly visible, E_{2g} and A_{1g} . The former mode is due to the in-plane vibrations of S atoms with respect to a Mo atom, and the latter is due to out-of-plane vibrations of S atoms [27]. The relative distance of these two peaks determine the number of layers of the MoS_2 flake [28]. The measured E_{2g} peak is located at 382.7 cm^{-1} for both OS and DS, and the A_{1g} peak at 403.5 and 403 cm^{-1} , which results in a relative peak distance equal to 20.8 and 20.3 cm^{-1} for OS and DS respectively, indicating a monolayer MoS_2 . To further confirm this result, AFM measurements are performed on several different triangular flakes from both OS and DS.

Fig. 4(a) and (c) show AFM images of the MoS_2 triangle presented at Fig. 2(a) of OS and a similarly large one of DS. Since the flakes are very large ($>300 \mu\text{m}$) they cannot entirely be scanned and visualized by our AFM system, thus they are only partially scanned at their border to measure the thickness of the MoS_2 layer. A section profile is further performed (see Fig. 4(b) and (d)), which reveals the thickness of the MoS_2 layer (height of layer compared to substrate level) and is equal to 0.76 and 0.68 nm for OS and DS respectively, indicating a monolayer. However, it can be seen that there is a region across the border of both

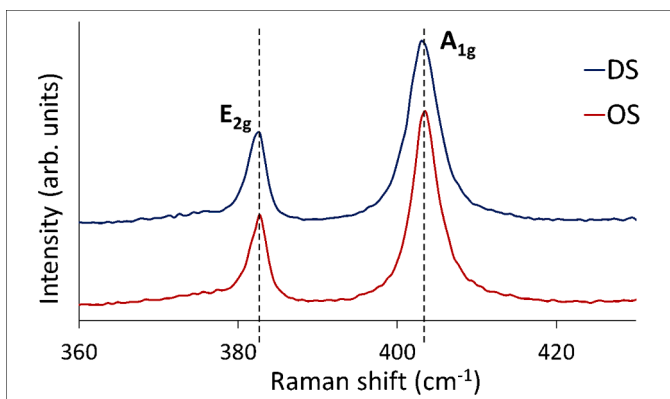


Fig. 3. Raman spectrum of a MoS_2 triangular flake of both OS and DS. The relative distance between the two peaks is equal to 20.8 and 20.3 cm^{-1} for OS and DS respectively.

flakes with a width of $\sim 700 \text{ nm}$, where the thickness is approximately double. Specifically, the thickness measured between the monolayer and the top of this elevated region is 0.84 and 0.81 nm (for OS and DS respectively), relatively equal to another monolayer of MoS_2 . Therefore, we speculate that this is due to folding of the flake at its borders, probably after the growth and during the cooling step which induces strain between the substrate and the MoS_2 layer due to different thermal expansion coefficients of the two materials.

Both Raman and AFM analyses demonstrate that our proposed growth method results in large triangular flakes which are monolayers. The grown MoS_2 flakes are similar in terms of quality with the flakes deposited using the conventional CVD-based growth method (i.e. few mg of MoO_3 powder as the Mo precursor) [15,17]. However, the flakes reported in this work appear to be larger compared to the ones deposited with conventional growth method [18-20], which can be beneficial for several different applications that require large active area for sensing and/or device fabrication.

3.3. Electrical characterization

The electrical characterization of a MoS_2 flake is performed by extracting current-voltage (I-V) measurements at a range of -2 to 2 V with 0.1 V step and at a temperature range of 80 to 300 K with 20 K step, using two probes. All measurements are done under vacuum conditions. In a two-probe configuration, the current is described by the following formula:

$$I = \frac{ah}{\rho s} V \quad (1)$$

where h is the thickness of the medium that the current is flowing through, a is the electrodes' width and s is the electrodes distance (see Fig. 5(a)). In our case, the total measured resistance is a series resistance of the MoS_2 resistance (R_{MoS_2}), the contact resistance between Ti/Au electrodes and MoS_2 (R_{contact1}), the contact resistance between the probes and the electrodes (R_{contact2}) and the connectors resistance (R_{wire}), as can be seen in Fig. 5(a). We can assume that R_{contact2} and R_{wire} is negligible. Moreover, the electrical contact between Ti/Au and MoS_2 is found to be ohmic and thus, R_{contact1} can also be neglected. Furthermore, the MoS_2 conductivity can be calculated by the following formula:

$$\sigma = (\rho)^{-1} = \left(R_{\text{MoS}_2} \frac{ah}{s} \right)^{-1} \quad (2)$$

The thickness of the MoS_2 flake (h) is measured to be $\sim 0.7 \text{ nm}$, the width of the electrodes (a) is $50 \mu\text{m}$ and the distance of the electrodes (s) is equal to $50 \mu\text{m}$. Fig. 5(c) shows an optical microscope image of a triangular MoS_2 flake with the formed Ti/Au electrodes on top.

Fig. 6(a) shows the temperature dependence of the MoS_2 flake conductance. As can be seen, the conductance is decreased as the temperature decreases which indicates the semiconducting behavior of the material. The conductance (and thus, the conductivity) exhibits a strong dependence with temperature, but at a certain temperature value (160 K) this dependence becomes weaker. The thermal activation energy can be extracted by the Arrhenius plot (Fig. 6(b)), by calculating the slope of the fitted straight line. However, one can see that the data points are best fitted using two separate straight lines of different slopes. This indicates that according to the temperature range, two different conduction mechanisms may dominate [29]. In the case of the "high" temperature range of 180 – 300 K , the conductivity is described by the following formula:

$$\sigma = \sigma_0 \exp\left(-\frac{E_a}{k_B T}\right) \quad (3)$$

where σ_0 is the conductivity at $T = 0 \text{ K}$, E_a is the thermal activation energy and k_B is Boltzmann constant. In such a case, the activation energy is indeed calculated by the slope of the line and is equal to 15.5

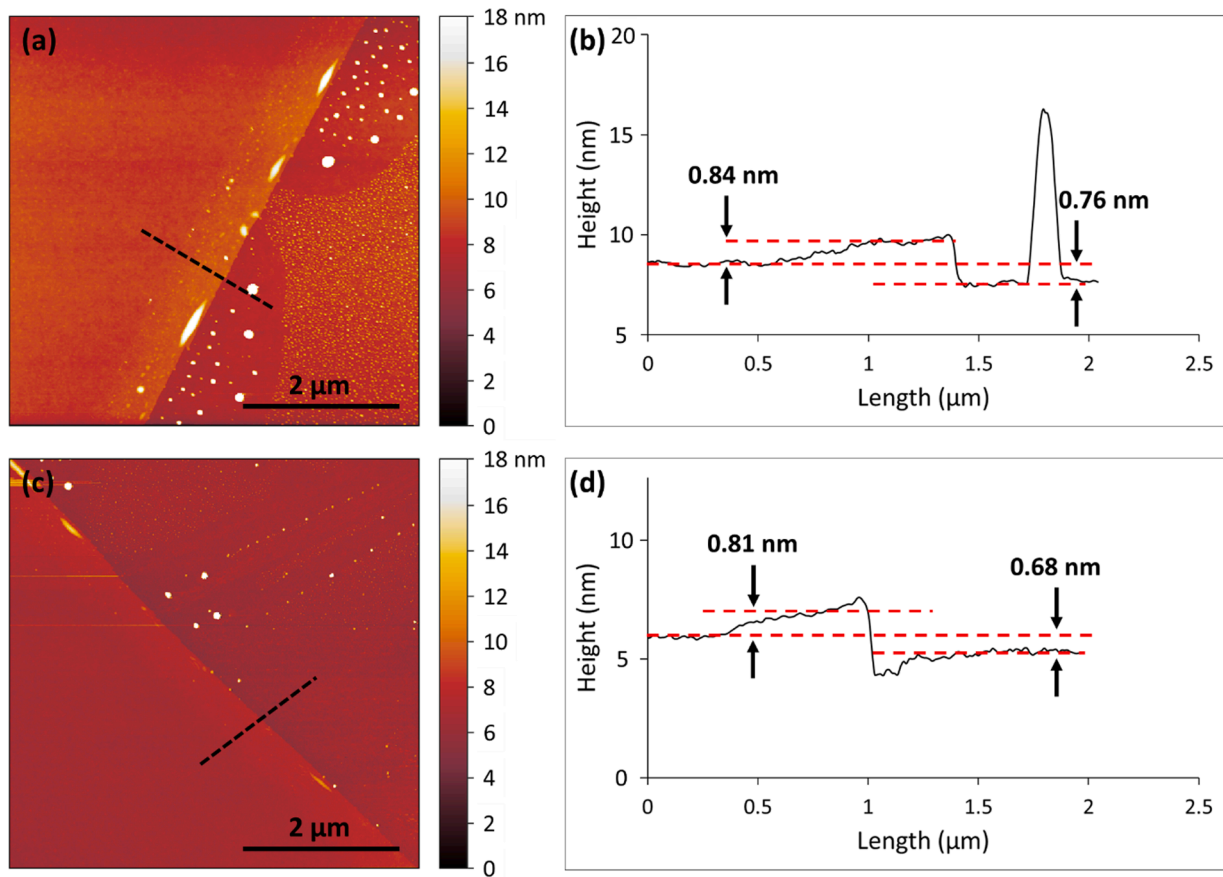


Fig. 4. (a) AFM image and (b) section profile as indicated by the dashed line of part of a triangular flake of OS. (c) AFM image and (d) section profile of part of a triangular flake of DS.

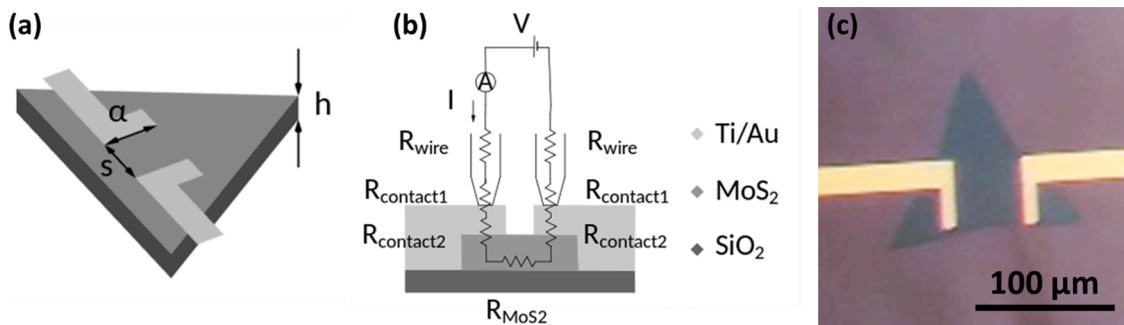


Fig. 5. (a) Sketch of the triangular flake of thickness h , with electrodes of width a and distance s , (b) sketch of the electrical circuit when the probes come in contact with the Ti/Au electrodes, (c) optical microscope image of the triangular MoS₂ flake with the formed electrodes on top of it.

meV. Our result is in good agreement with previously reported E_a values at this temperature range [29,30].

At the “low” temperature range of 80–160 K, the conductivity is described by the formula:

$$\sigma = \sigma_0 \exp \left[- \left(\frac{T_0}{T} \right)^{1/(1+d)} \right] \quad (4)$$

according to Mott’s variable range hopping (VRH) model [31,32], where T_0 is the characteristic temperature and d the dimensionality of the system (equal to 2 for a 2D material). Therefore, the exponent of Eq. (4) is equal to 1/3 and T_0 is found to be $6 \cdot 10^3$ K, based on the slope of the fitted straight line shown in Fig. 6(c). This conduction mechanism model has been previously proposed for MoS₂ nanoflakes, and accurately describes the transport mechanism of the 2D material at low temperatures

[33,34].

Therefore, we conclude that the conductivity is more sensitive in temperature changes at higher temperatures (180–300 K), and is dominated by nearest-neighbor hopping mechanism. As the temperature decreases (<180 K), charge carriers will more probably hop over longer distances that have closer energy spacing, which indicates that the dominant conduction mechanism is Mott’s VHR [35].

Furthermore, a back-gate Ag electrode is formed at the back side of the sample by scratching the back surface and pouring a small amount of Ag paste. Then, I-V measurements are performed between the two electrodes (drain/source) at a range of 0 to 1 V with 0.1 V step and at room temperature, while applying a gate voltage (V_g) at a range of 0 to 70 V with 10 V step. Such high V_g values are necessary in order to obtain gate action for a 300 nm thick SiO₂ film. Fig. 7(a) shows the drain-source

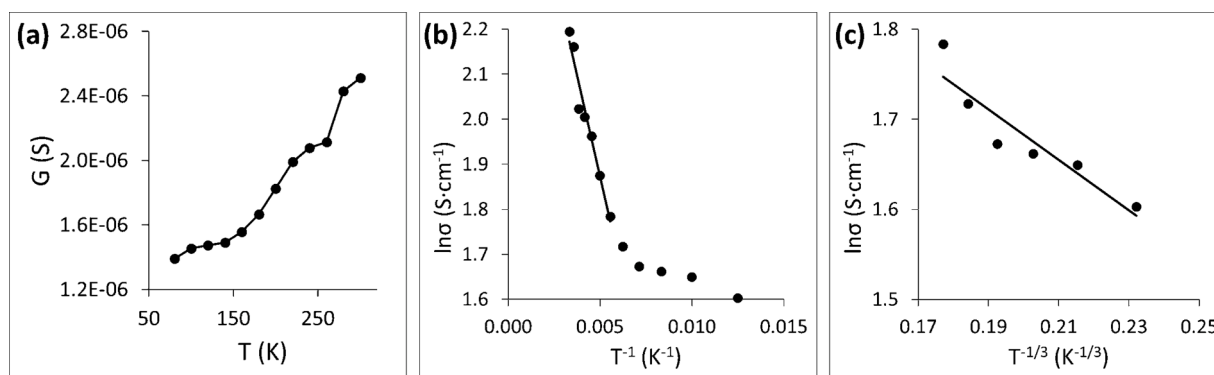


Fig. 6. (a) Temperature dependence of conductance, (b) variation of $\ln\sigma$ with $1/T$, fitting is performed for temperatures between 180 and 300 K, and (c) variation of $\ln\sigma$ with $1/(T^{1/3})$, fitting is performed for temperatures between 80 and 160 K.

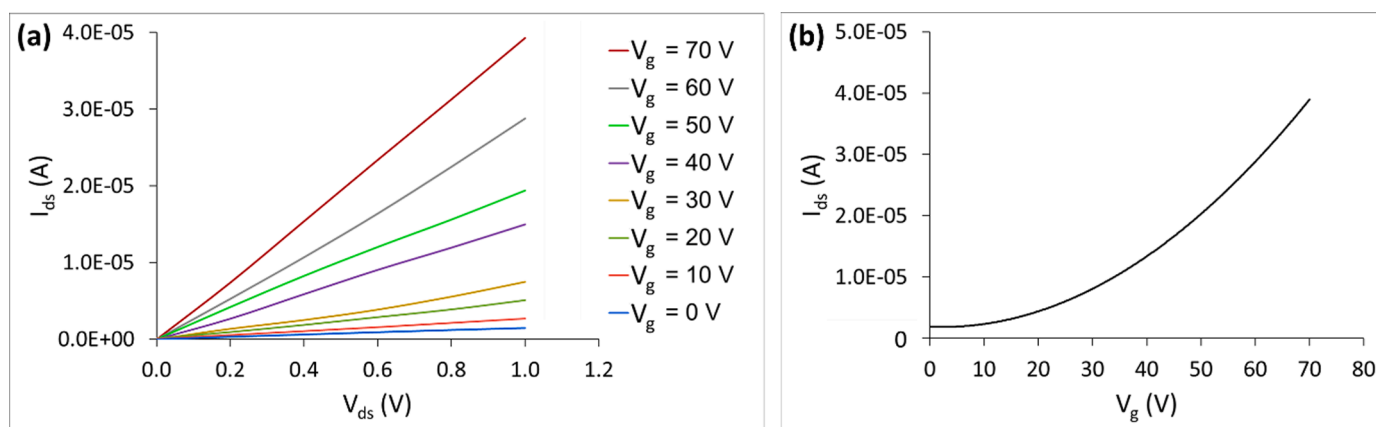


Fig. 7. (a) I_{ds} - V_{ds} characteristics for different applied V_g values. (b) I_{ds} dependence with V_g .

current-voltage (I_{ds} - V_{ds}) characteristics for different V_g values, indicating the clear dependence of the current flow between source-drain electrodes with the applied gate voltage. Fig. 7(b) demonstrates the I_{ds} dependence with V_g . The field effect mobility μ can be calculated by the following formula [36,37]:

$$\mu = \frac{dI_{ds}}{dV_g} \times \frac{s}{\alpha C_{ox} V_{ds}}$$

where s and α are the electrodes' (drain/source) distance and length respectively and equal to $50 \mu\text{m}$ for both values as denoted previously, $C_{ox}=1.2 \cdot 10^{-4} \text{ F m}^{-2}$ and dI_{ds}/dV_g is calculated by the slope of the curve shown in Fig. 7(b) for V_g values between 50 and 70 V. The calculated mobility at 300 K is equal to $0.9 \text{ cm}^2 \text{ V}^{-1} \text{ s}^{-1}$ which is comparable to the $0.1 - 10 \text{ cm}^2 \text{ V}^{-1} \text{ s}^{-1}$ range reported in the literature for monolayer MoS₂ [37-39].

4. Conclusions

In this work, we present a substrate capping technique for the growth of large monolayer MoS₂ flakes, which are uniformly formed over the entire substrate surface. The combination of two "sandwiched" substrate pieces with a Mo-based liquid precursor has been proven to produce two almost identical samples consisting of large (up to $>300 \mu\text{m}$) MoS₂ flakes, which are homogeneously covering the entire substrate surface at a relative uniform order. Moreover, Raman and AFM analysis demonstrate that the grown material is a monolayer. Low-temperature electrical characterization indicates that our MoS₂ flakes exhibit a semiconducting behavior. Further analysis of the results reveal two conduction mechanisms according to the measurement temperature

range, the nearest-neighbor hopping mechanism for high temperatures (180–300 K) and Mott's variable-range hopping mechanism for low temperatures (80–160 K). Future work includes further optimization of this method in order to obtain a fully closed MoS₂ film with a low grain-boundary area (thus, with even larger triangular flakes merged with each other), which is highly attractive in many different applications such as transistors and sensors, among others.

CRediT authorship contribution statement

Menelaos Tsigkourakos: Conceptualization, Methodology, Data curation, Writing - original draft. **Maria Kainourgiaki:** Data curation, Methodology, Validation, Formal analysis, Investigation. **Evangelos Skotadis:** Methodology, Investigation. **Konstantinos P. Giannakopoulos:** Writing - review & editing. **Dimitris Tsoukalas:** Conceptualization, Supervision. **Yannis S. Raptis:** Writing - review & editing.

Declaration of Competing Interest

The authors declare that they have no known competing financial interests or personal relationships that could have appeared to influence the work reported in this paper.

Acknowledgements

This research is funded in the context of the project "Development of low-dimensional material-based biosensor for DNA detection" (MIS 5049088) under the call for proposals "Researchers' support with an emphasis on young researchers- 2nd Cycle". The project is co-financed by Greece and the European Union (European Social Fund- ESF) by

the Operational Programme Human Resources Development, Education and Lifelong Learning 2014–2020.

References

- [1] O. El Beqqali, I. Zorkani, F. Rogemond, Chermette H, r.Ben Chaabane, M. Gamoudi, G. Guillaud, Electrical properties of molybdenum disulfide MoS₂. Experimental study and density functional calculation results, *Synth. Met.* 90 (1997) 165–172.
- [2] R. Ganatra, Q. Zhang, Few-layer MoS₂: a promising layered semiconductor, *ACS Nano* 8 (2014) 4074–4099.
- [3] A. Molina-Sanchez, K. Hummer, L. Wirtz, Vibrational and optical properties of MoS₂: from monolayer to bulk, *Surf. Sci. Rep.* 70 (2015) 554–586.
- [4] G.A. Ermolaev, Y.V. Stebunov, A.A. Vyshnevyy, D.E. Tatarikin, D.I. Yakubovskiy, S. M. Novikov, D.G. Baranov, T. Shegai, A.Y. Nikitin, A.V. Arsenin, V.S. Volkov, Broadband optical properties of monolayer and bulk MoS₂, *NPJ 2D Mater. Appl.* 4 (2020) 21.
- [5] J. Wu, P. Cao, Z. Zhang, F. Ning, S.-S. Zheng, J. He, Z. Zhang, Grain-size-controlled mechanical properties of polycrystalline monolayer MoS₂, *Nano Lett.* 18 (2018) 1543–1552.
- [6] J.-W. Jiang, H.S. Park, Mechanical properties of MoS₂/graphene heterostructures, *Appl. Phys. Lett.* 105 (2014), 033108.
- [7] D. Seo, D.Y. Lee, J. Kwon, J.J. Lee, T. Taniguchi, K. Watanabe, G.-H. Lee, K.S. Kim, J. Hone, Y.D. Kim, H.-J. Choi, High-performance monolayer MoS₂ field-effect transistor with large-scale nitrogen-doped graphene electrodes for Ohmic contact, *Appl. Phys. Lett.* 115 (2019), 012104.
- [8] H. Kwon, S. Garg, J.H. Park, Y. Jeong, S. Yu, S.M. Kim, P. Kung, S. Im, Monolayer MoS₂ field-effect transistors patterned by photolithography for active matrix pixels in organic light-emitting diodes, *NPJ 2D Mater. Appl.* 3 (2019) 1–9.
- [9] D.-W. Lee, J. Lee, I.Y. Sohn, B.-Y. Kim, Y.M. Son, H. Bark, J. Jung, M. Choi, T. H. Kim, C. Lee, N.-E. Lee, Field-effect transistor with a chemically synthesized MoS₂ sensing channel for label-free and highly sensitive electrical detection of DNA hybridization, *Nano Res* 8 (2015) 2340–2350.
- [10] J. Park, J. Mun, J.-S. Shin, S.-W. Kang, Highly sensitive two-dimensional MoS₂ gas sensor decorated with Pt nanoparticles, *R. Soc. Open Sci.* 5 (2018), 181462.
- [11] M. Park, Y.J. Park, X. Chen, Y.-K. Park, M.-S. Kim, J.-H. Ahn, MoS₂-based tactile sensor for electronic skin applications, *Adv. Mater.* 28 (2016) 2556–2562.
- [12] A. Arab, Q. Li, Anisotropic thermoelectric behavior in armchair and zigzag mono- and fewlayer MoS₂ in thermoelectric generator applications, *Sci. Rep.* 5 (2015) 13706.
- [13] H. Li, J. Wu, Z. Yin, H. Zhang, Preparation and applications of mechanically exfoliated single-layer and multilayer MoS₂ and WSe₂ nanosheets, *Acc. Chem. Res.* 47 (2014) 1067–1075.
- [14] H. Lin, J. Wang, Q. Luo, H. Peng, C. Luo, R. Qi, R. Huang, J. Travas-Sejdic, C.-G. Duan, Rapid and highly efficient chemical exfoliation of layered MoS₂ and WS₂, *J. Alloys Compd.* 699 (2017) 222–229.
- [15] Y.-H. Lee, X.-Q. Zhang, W. Zhang, M.-T. Chang, C.-T. Lin, K.-D. Chang, Y.-C. Yu, J.T.-W. Wang, C.-S. Chang, L.-J. Li, T.-W. Lin, Synthesis of large-area MoS₂ atomic layers with chemical vapor deposition, *Adv. Mater.* 24 (2012) 2320–2325.
- [16] Y. Zhan, Z. Liu, S. Najmaei, P.M. Ajayan, J. Lou, Large-area vapor-phase growth and characterization of MoS₂ atomic layers on a SiO₂ substrate, *Small* 8 (2012) 966–971.
- [17] S.H. Baek, Y. Choi, W. Choi, Large-area growth of uniform single-layer MoS₂ thin films by chemical vapor deposition, *Nanoscale Res. Lett.* 10 (2015) 388.
- [18] S. Wang, Y. Rong, Y. Fan, M. Pacios, H. Bhaskaran, K. He, J.H. Warner, Shape evolution of monolayer MoS₂ crystals grown by chemical vapor deposition, *Chem. Mater.* 26 (2014) 6371–6379.
- [19] N. Kumar, R. Tomar, N. Wadehra, M.M. Devi, B. Prakash, S. Chakraverty, Growth of highly crystalline and large scale monolayer MoS₂ by CVD: the role of substrate position, *Cryst. Res. Technol.* 53 (2018), 1800002.
- [20] A. Özden, F. Ay, C. Sevik, N.K. Perkgöz, CVD growth of monolayer MoS₂: role of growth zone configuration and precursors ratio, *Jpn. J. Appl. Phys.* 56 (2017) 06GG05.
- [21] X. Ling, Y.-H. Lee, Y. Lin, W. Fang, L. Yu, M.S. Dresselhaus, J. Kong, Role of the seeding promoter in MoS₂ growth by chemical vapor deposition, *Nano Lett* 14 (2014) 464–472.
- [22] A. Michail, J. Parthenios, D. Anastopoulos, C. Galiotis, M. Christian, L. Ortolani, V. Morandi, K. Papagelis, Controllable, eco-friendly, synthesis of highly crystalline 2D-MoS₂ and clarification of the role of growth-induced strain, *2D Mater* 5 (2018), 035035.
- [23] S. Li, Y.-C. Lin, X.-Y. Liu, Z. Hu, J. Wu, H. Nakajima, S. Liu, T. Okazaki, W. Chen, T. Minari, Y. Sakuma, K. Tsukagoshi, K. Suenaga, T. Taniguchi, M. Osada, Wafer-scale and deterministic patterned growth of monolayer MoS₂ via vapor–liquid–solid method, *Nanoscale* 11 (2019) 16122–16129.
- [24] X. Zhang, H. Nan, S. Xiao, X. Wan, Z. Ni, X. Gu, K. Ostrikov, Shape-uniform, high-quality monolayered MoS₂ crystals for gate-tunable photoluminescence, *ACS Appl. Mater. Interfaces* 9 (2017) 42121–42130.
- [25] S. Zhou, L. Gan, D. Wang, H. Li, T. Zhai, Space-confined vapor deposition synthesis of two dimensional materials, *Nano Res* 11 (2018) 2909–2931.
- [26] P.K. Mohapatra, S. Deb, B.P. Singh, P. Vasa, S. Dhara, Strictly monolayer large continuous MoS₂ films on diverse substrates and their luminescence properties, *Appl. Phys. Lett.* 108 (2016), 042101.
- [27] K. Golas, R.Bozek M.Grzeszczyk, A.Wysmolek P.Leszczynski, A.Babinski M. Potemski, Resonant Raman scattering in MoS₂-From bulk to monolayer, *Solid State Commun* 197 (2014) 53–56.
- [28] H. Li, Q. Zhang, C.C.R. Yap, B.K. Tay, T.H.T. Edwin, A. Olivier, D. Baillargeat, From bulk to monolayer MoS₂: evolution of Raman scattering, *Adv. Funct. Mater.* 22 (2012) 1385–1390.
- [29] M.D. Siao, W.C. Shen, R.S. Chen, Z.W. Chang, M.C. Shih, Y.P. Chiu, C.-M. Cheng, Two-dimensional electronic transport and surface electron accumulation in MoS₂, *Nat. Commun.* 9 (2018) 1442.
- [30] B. Radisavljevic, A. Kis, Mobility engineering and a metal–insulator transition in monolayer MoS₂, *Nat. Mater.* 12 (2013) 815–820.
- [31] K. Hippalgaonkar, Y. Wang, Y. Ye, D.Y. Qiu, H. Zhu, Y. Wang, J. Moore, S.G. Louie, X. Zhang, High thermoelectric power factor in two-dimensional crystals of MoS₂, *Phys. Rev. B* 95 (2017), 115407.
- [32] S. Ghatak, A.N. Pal, A. Ghosh, Nature of electronic states in atomically thin MoS₂ field-effect transistors, *ACS Nano* 5 (2011) 7707–7712.
- [33] J. Xue, S. Huang, J.-Y. Wang, H.Q. Xu, Mott variable-range hopping transport in a MoS₂ nanoflake, *RSC Adv.* 9 (2019) 17885–17890.
- [34] D. Jariwala, V.K. Sangwan, D.J. Late, J.E. Johns, V.P. Dravid, T.J. Marks, L. J. Lauhon, M.C. Hersam, Band-like transport in high mobility unencapsulated single-layer MoS₂ transistors, *Appl. Phys. Lett.* 102 (2013), 173107.
- [35] H. Qiu, T. Xu, Z. Wang, W. Ren, H. Nan, Z. Ni, Q. Chen, S. Yuan, F. Miao, F. Song, G. Long, Y. Shi, L. Sun, J. Wang, X. Wang, Hopping transport through defect-induced localized states in molybdenum disulfide, *Nat. Commun.* 4 (2013) 2642.
- [36] X. Liu, J. He, Q. Liu, D. Tang, J. Wen, W. Liu, W. Yu, J. Wu, Z. He, Y. Lu, D. Zhu, W. Liu, P. Cao, S. Han, K.-W. Ang, Low temperature carrier transport study of monolayer MoS₂ field effect transistors prepared by chemical vapor deposition under an atmospheric pressure, *J. Appl. Phys.* 118 (2015), 124506.
- [37] W. Wu, D. De, S.-C. Chang, Y. Wang, H. Peng, J. Bao, S.-S. Pei, High mobility and high on/off ratio field-effect transistors based on chemical vapor deposited single-crystal MoS₂ grains, *Appl. Phys. Lett.* 102 (2013), 142106.
- [38] B. Radisavljevic, A. Radenovic, J. Brivio, V. Giacometti, A. Kis, *Nat. Nanotechnol.* 6 (2011) 147–150.
- [39] Z. Yu, Z.-Y. Ong, S. Li, J.-B. Xu, G. Zhang, Y.-W. Zhang, Y. Shi, X. Wang, *Adv. Funct. Mater.* 27 (2017), 1604093.